

# Gaia DR3 Variable White Dwarfs vetted by ZTF

Timour Jestin<sup>1</sup>, Thịnh Hữu Nguyẽn<sup>2,3</sup>, Laurent Eyer<sup>1</sup>, Lorenzo Rimoldini<sup>4</sup>, Ashish Mahabal<sup>5</sup>, Marc Audard<sup>1</sup>, Pedro García-Lario<sup>6</sup>, Panagiotis Gavras<sup>7</sup>, and Krzysztof Nienartowicz<sup>4,8</sup>

<sup>1</sup> Department of Astronomy, University of Geneva, Chemin Pegasi 51, 1290 Versoix, Switzerland

<sup>2</sup> Department of Astronomy, University of Illinois Urbana-Champaign, 1002 W. Green Street, Urbana, IL, 61801, USA

<sup>3</sup> Department of Astrophysics and Planetary Sciences, Villanova University, 800 E. Lancaster Avenue, Villanova, PA, 19085, USA

<sup>4</sup> Department of Astronomy, University of Geneva, Chemin d'Ecogia 16, 1290 Versoix, Switzerland

<sup>5</sup> Division of Physics, Mathematics, and Astronomy, California Institute of Technology, Pasadena, CA 91125, USA

<sup>6</sup> European Space Astronomy Centre (ESA/ESAC), Villanueva de la Canada, 28692 Madrid, Spain

<sup>7</sup> Starion for European Space Agency (ESA), Camino bajo del Castillo, s/n, Urbanizacion Villafranca del Castillo Villanueva de la Cañada, 28692 Madrid, Spain

<sup>8</sup> Sednai Sarl, Rue des Marbriers 4, 1204 Geneva, Switzerland

September 19, 2025

## ABSTRACT

**Context.** The publications of *Gaia* DR2 and DR3 have brought major improvements in stellar astrometry and photometry, particularly regarding the description of the white dwarf sequence. In particular, *Gaia* DR2 enabled the detection of variability in white dwarfs based solely on averaged astrometric and photometric quantities, i.e. the astrometric 5 parameters (positions, proper motion, and parallax) and general photometry properties in the G, BP and RP bands (mean, standard deviation and number of measurements).

**Aims.** We identify and classify variable white dwarfs using *Gaia* DR3 data and Zwicky Transient Facility (ZTF) DR23 observations. The objective is to construct a catalogue of pulsating white dwarf candidates with robust selection criteria.

**Methods.** We define a new sample of candidate variable white dwarfs using *Gaia* DR3 astrometric and photometric data. We cross-match this sample with the ZTF DR23 catalogue and apply a multiband Lomb-Scargle periodogram analysis to detect periodic variability. We then use the OPTICS unsupervised clustering algorithm to group and classify the confirmed periodic stars.

**Results.** We identify 1423 variable white dwarfs candidates from *Gaia* DR3, with 864 having ZTF time series. Among these, 141 present significant periodicity. Using unsupervised clustering techniques, we classify these objects into known categories, including ZZ Ceti stars, GW Vir, V777 Her, and white dwarf–main sequence (WD–MS) binaries. Our analysis reveals several confirmed periodic stars, including three ZZ Ceti stars, 15 GW Vir stars, one V777 Her, and 24 WD–MS binaries. Furthermore, it reveals a significant population of potentially variable stars, even though without confirmed periodicity. Finally several variables show unusual properties and are highlighted for follow-up studies.

**Conclusions.** Our catalogue of candidate variable white dwarfs includes variability status, periodicity, and classification information for the 864 sources with ZTF time series, 519 of them newly identified (including 83 new periodic stars). It is publicly available through the VizieR database to support future investigations of white dwarf variability.

**Key words.** Variable stars(1761), White dwarf stars(1799)

## 1. Introduction

We are in an epoch of enormous data growth in optical astronomy. The challenge lies not only in the increase in data volume, but also in the variety of survey properties and data types. Among all astronomical surveys, the *Gaia* mission (Gaia Collaboration et al. 2016b), a cornerstone of the ESA science program launched in late 2013, is unique. From a single space-based platform, it delivered repeated astrometric, photometric, spectrophotometric, and spectroscopic measurements over the entire celestial sphere for more than 10 years.

The *Gaia* DPAC consortium (Mignard et al. 2008) has taken care of the data reduction, calibration and analysis of the *Gaia* data and has also prepared the data products to be published by ESA in a stepwise manner. This approach aims to improve the data reduction, lower random and systematic errors in all data products, and gradually increase the number of published sources and data products. The same iterative approach was followed for publishing the *Gaia* photometric time series. For the first *Gaia* Data Release (Septem-

ber 2016; Gaia Collaboration et al. 2016a; Eyer et al. 2017), a selection of 3,194 variable stars near the South Ecliptic pole that partially covers the Large Magellanic Cloud was published with their G-band time series. With *Gaia* DR2 (April 2018; Gaia Collaboration et al. 2018), more than half a million variable objects were published with their G, integrated BP, and RP time series. *Gaia* DR3 (Gaia Collaboration et al. 2022, 2021; Eyer et al. 2023; Riello et al. 2021) then released the G, BP and RP epoch photometry of some 11.7 million sources. This represents one of the largest published catalogues for many variability types (such as, RR Lyrae stars, large-amplitude long-period variable stars,  $\delta$  Scuti stars).

Furthermore, a performance verification paper (Gaia Collaboration et al. 2019, published as companion to *Gaia* DR2) describes the variability across the observational Hertzsprung-Russell (HR) diagram, notably including distinctive variability features in the white dwarf sequence.

Within *Gaia* data, the published averaged statistics can help infer the variability of stars whose time series have not been re-

leased (for example, Belokurov et al. 2017; Mowlavi et al. 2021; Guidry et al. 2021; Maíz Apellániz et al. 2023). Using the relationship between the uncertainty of the mean and its associated standard deviation, corrected for an estimation of the instrumental and photon noises (Eyer 1998), it is possible to study the variability of certain HR regions with a comprehensive approach. Notably, Eyer et al. (2020) explored the variability of the white dwarfs identified by Gentile Fusillo et al. (2019).

The aim of this article is to study variable white dwarfs, which are selected from the Gentile Fusillo et al. (2021) white dwarf catalogue, using *Gaia* DR3 and the Zwicky Transient Facility (ZTF) DR23 data (Bellm et al. 2019; Masci et al. 2018) as well as to compare the candidates with the literature. We aim to present a list of pulsating white dwarf candidates with adjusted criteria employing *Gaia* DR3 measurements while also considering other variable types. A systematic search for variability in white dwarfs is particularly valuable, as it can reveal insights into their physical properties, especially for those located in specific locations in the HR diagram, such as the crystallisation sequence.

The article is structured as follows. First, we present some general properties of the *Gaia* and ZTF surveys in Section 2. In Section 3, we show the criteria used to select and refine eligible variable white dwarf candidates from *Gaia* DR3. After obtaining the list of candidates, we describe our procedure to cross-match with ZTF data and extract the frequency from the time series in Section 4. Then, Section 5 presents our selection of pulsating white dwarf candidates. We also classify these candidates using unsupervised clustering, and cross-match them with known stars from the literature.

## 2. Data

In this study, we use *Gaia* DR3 and ZTF DR23 data obtained from their respective public archives<sup>1,2</sup>. We use the *Gaia* photometry (Evans et al. 2018; Riello et al. 2021) and astrometry (Lindegren et al. 2018, 2021) measurements to determine our targets' locations in the Hertzsprung-Russell (HR) Diagram. The ZTF time series in the *g* and *r* bands (referred to as *Zg* and *Zr* respectively) are then used to determine potential periodic stars among our candidates.

Using a random sample of about 3000 white dwarf candidates from Gentile Fusillo et al. (2021)'s *Gaia* DR3 catalogue that have ZTF time series, we study the general properties of the *Gaia* and ZTF observations. Fig. 1 displays the number of epochs observed in each band of *Gaia* DR3 and ZTF DR23. These are defined as the number of Field-of-View (FoV) transits for *Gaia*, and the number of observations for ZTF. The sources have a lower number of observed epochs in *Gaia* DR3 compared to ZTF DR23, with a median number of observed epochs of 41, 33, and 34, in *Gaia*'s G, RP, and BP bands respectively, while these reach 129 in the *Zg* band and 190 in the *Zr* band. While the ZTF data yields higher noise per measurement than *Gaia*, the higher number of measurements should allow for comparable error levels on the mean magnitudes.

We then compare the standard deviation of the time series  $\sigma(G)$  and the error of the mean magnitude  $\sigma(\bar{G})$  between the two datasets. For *Gaia* data, these are estimated using the number of observations per CCD (`phot_g_n_obs`) and the photometric mean flux over its error (`phot_g_mean_flux_over_error`):

$$\sigma(G) = \frac{2.5}{\ln 10} \cdot \frac{\sqrt{\text{phot\_g\_n\_obs}}}{\text{phot\_g\_mean\_flux\_over\_error}}, \quad (1)$$

$$\sigma(\bar{G}) = \frac{2.5}{\ln 10} \cdot \frac{1}{\text{phot\_g\_mean\_flux\_over\_error}}. \quad (2)$$

For the ZTF data,  $\sigma(\bar{G})$  is calculated by dividing the time series standard deviation by the square root of the number of measurements in the *Zg* band. Figure 2 displays the error of the mean magnitude as a function of the mean magnitude in the G resp. *Zg* bands, computed on our previous star sample. It demonstrates that both *Gaia* and ZTF have comparably low noise (below 10 milli-mag, for  $G < 18$ ) and confirms that ZTF data can be used to detect periodic signal from *Gaia*'s variable white dwarf candidates even when photometric time series are unavailable in *Gaia*. Moreover, ground-based surveys like ZTF typically have a spectral window with peaks around multiples of 1 cycle per day. In the case of *Gaia*, the period of rotation is 6 hours, inducing peaks at multiples of 4 cycles per day. This difference in survey cadence can lift aliasing ambiguities when combining the two surveys.

## 3. Selecting *Gaia* DR3 variable white dwarf candidates

### 3.1. Candidacy criteria

We obtained our variable white dwarf candidates from Gentile Fusillo et al. (2021)'s *Gaia* DR3 white dwarf catalogue. Even though these stars have already been selected using strict quality criteria on both photometric and astrometric flags, we decided to take stricter and more conservative restrictions to avoid contamination for our subsequent selection. In particular, dimmer sources (as shown in Figure 2) and sources with a high colour index likely exhibit large photometric variability due to noise rather than intrinsic variability. Thus, we impose our own restrictions on these parameters:

$$\begin{aligned} P_{WD} &\geq 0.75, \\ \text{phot\_g\_mean\_mag} &< 18, \\ \text{phot\_bp\_mean\_mag} - \text{phot\_rp\_mean\_mag} &\leq 2, \\ \text{astrometric\_excess\_noise\_sig} &\leq 15, \end{aligned} \quad (3)$$

where  $P_{WD}$  is the probability of being a white dwarf calculated by Gentile Fusillo et al. (2021) and the rest are the *Gaia* parameters. We also want to note that these restrictions are empirical and are selected based on the cleanliness of the resulting overdensity regions later on. These limits may exclude true variable sources but are essential to ensure the purity of the selection. This filtering reduces the selection from  $\sim 1.3$  million stars in the initial catalogue, to 22264 sources.

Next, we assess the variability of our remaining sources. Figure 3 displays the *G*-band estimated standard deviation of the time series per CCD (from Equation (1)) as a function of the mean *Gaia* *G*-band magnitude,  $\bar{G}$ . The relationship between noise and mean magnitude is fitted as an exponential function  $f(\bar{G}) = \exp(a \cdot \bar{G} + b) + c$  using SciPy's `curve_fit` function (Virtanen et al. 2020). This yields:

$$\begin{aligned} \sigma(G; \bar{G}) &= \exp((7.48 \pm 0.01) \cdot 10^{-1} \cdot \bar{G} - 18.597 \pm 0.025) \\ &+ (3.8 \pm 0.1) \cdot 10^{-3} \end{aligned} \quad (4)$$

<sup>1</sup> <https://gea.esac.esa.int/archive/>

<sup>2</sup> <https://irsa.ipac.caltech.edu/Missions/ztf.html>

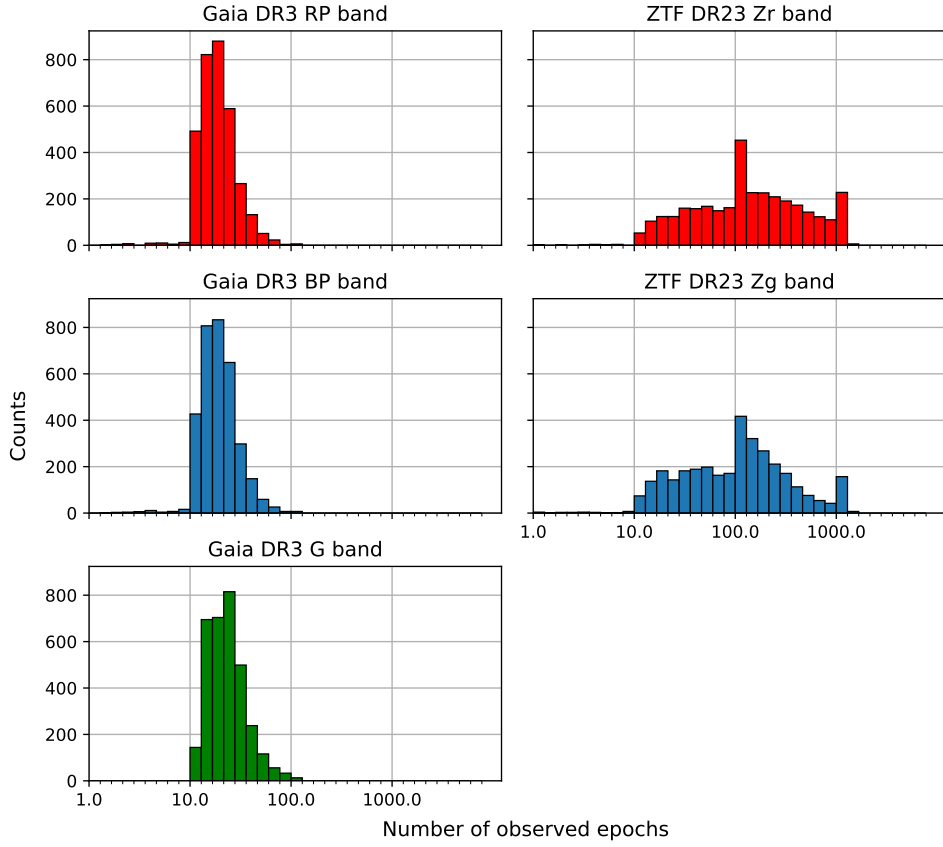


Fig. 1: These histograms display the number of observed epochs in each band for each survey. We randomly choose 3000 white dwarf candidates and extract their number of measurements in the two surveys. On average, ZTF DR23 has a greater number of observations per star than the number of FoV transits per star from *Gaia* DR3.

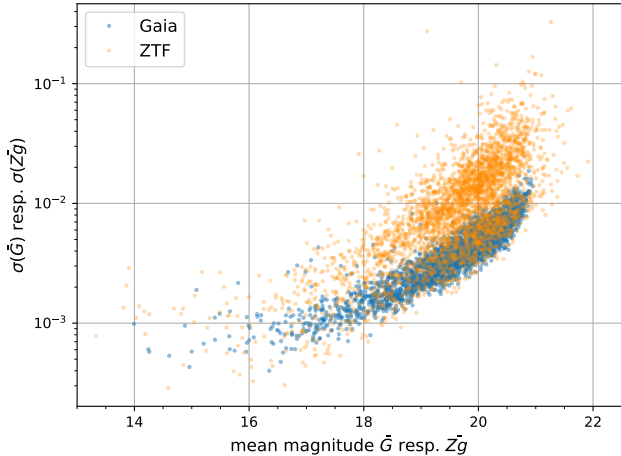


Fig. 2: We compare the error of the mean magnitude  $\sigma$  as a function of the mean magnitude of *Gaia* DR3 (G band) and ZTF DR23 time series (Zg band) for individual sources. Around 3000 white dwarf candidates are chosen randomly from the Gentile Fusillo et al. (2021) catalogue to measure the standard deviation of the mean magnitude. As *Gaia* yields very high precision for individual measurements and ZTF has many measurements, both surveys present low noise for their mean magnitude.

With the notation  $\sigma(G; \bar{G}) \equiv \sigma(G)$  used for clarity. This noise level corresponds to the average  $\sigma(G)$  for objects with constant magnitude. We then define a threshold to define our candidate variable stars as:

$$\text{variability threshold} = 1.25 \cdot \sigma(G; \bar{G}) \quad (5)$$

i.e. a 25% increase of the required  $\sigma(G)$  compared to its average value, reducing our selection to 1423 variable white dwarf candidates.

We present an HR diagram of our variable candidates in Figure 4. Along the white dwarf sequence, there are noticeable clumps. In particular, the ZZ Ceti clump ( $\text{BP-RP} \in [0, 0.1]$ , absolute  $G \in [11.6, 12.1]$ ), a potential V777 Her clump ( $\text{BP-RP} \in [-0.35, -0.25]$ , absolute  $G \in [10, 11]$ ), and potential GW Vir stars ( $\text{BP-RP} \in [-0.45, -0.4]$ , absolute  $G \in [8, 9]$ ).

### 3.2. Comparison with *Gaia* DR3 variability classifier

We compare our sample of candidate variable white dwarfs with the *Gaia* DR3 Machine Learning variability classification (Eyer et al. 2023; Rimoldini et al. 2023). This comparison then allows us to validate our candidacy criteria and can reveal possible missing sources in the *Gaia* classification algorithm. This yields: 994 (69.9%) unclassified candidates, 408 (28.7%) classified as white dwarfs, 8 as cataclysmic variables, 6 as eclipsing binaries, 5 as short time-scale variable stars and, most surprisingly, two RR Lyrae stars (*Gaia* DR3 3345661467822106624 and *Gaia* DR3 6555925496084361344). The two RR Lyrae are

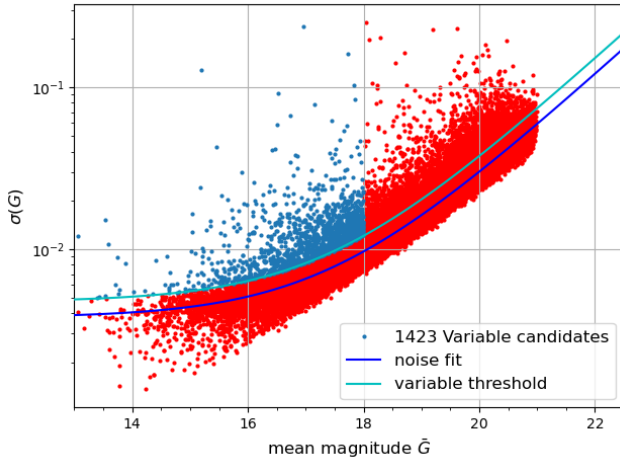


Fig. 3: The estimated standard deviation of the  $G$ -band per CCD time series, see Equation (1), plotted as a function of the mean magnitude  $\bar{G}$ . To select the variable white dwarf candidates, we use a threshold that is 25% higher than the computed noise function. In this selection, 1423 white dwarfs are variable candidates according to *Gaia* DR3 data.

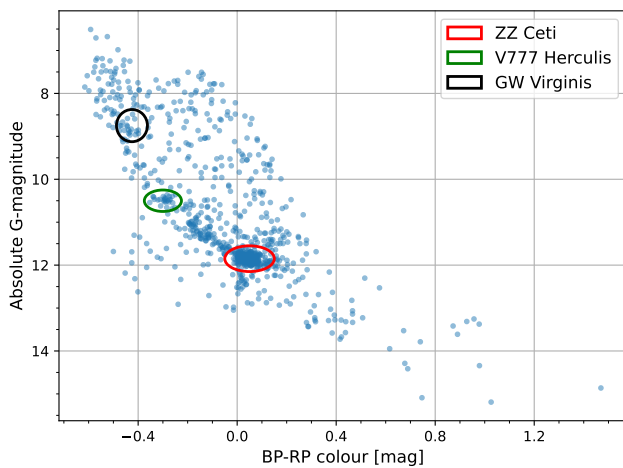


Fig. 4: HR diagram of our selection of variable white dwarf candidates from Figure 3. The potential ZZ Ceti, V777 Herculis and GW Virginis clumps are outlined by ellipses. We use the mean magnitude in the *Gaia*  $G$ ,  $BP$ , and  $RP$  bands.

most likely misclassifications, as they are not located in the horizontal branch stars, as would be expected for such stars.

## 4. Period search with ZTF data

### 4.1. Evaluating the ZTF cross-match query

ZTF data is cross-matched with *Gaia* by spatial constraint with a cone search of radius 10 arcsec. Each cross-match must have time series in both bands ( $Zg$  and  $Zr$ ) and have at least 20 measurements per band. If multiple objects match the query constraint, the closest positional match will be selected. This selection is enabled automatically by the *One to One Match* option in the ZTF archive. Among our 1423 variable white dwarf candidates, there are 894 stars with ZTF data available in both bands. However, wrong cross-matches can still happen, and additional

steps to check the query are necessary. To detect potential erroneous cross-matches, we examine each data point's Euclidean distance between the residuals of three linear regressions: the angular distance between *Gaia* and ZTF coordinates versus *Gaia* proper motion, the  $Zg$  mag versus *Gaia* BP mag, and the  $Zr$  mag versus *Gaia* RP mag. The linear functions are fitted using SciPy's `curve_fit`, and shown in Figure 5. The computed relationships are:

$$\begin{aligned}\hat{\theta} &= (2.168 \pm 0.160) \cdot 10^{-3} \mu + (112.6 \pm 18.0) \cdot 10^{-3} \\ \hat{Zg} &= (0.974 \pm 0.016) \cdot BP + (0.337 \pm 0.266) \\ \hat{Zr} &= (0.983 \pm 0.021) \cdot RP + (0.346 \pm 0.352)\end{aligned}\quad (6)$$

in which  $\theta$  is the angular distance (in arcseconds) between *Gaia* and ZTF coordinates,  $\mu$  is the *Gaia* DR3 proper motion (in milliarcseconds per year),  $Zg$  and  $Zr$  are the ZTF magnitude measurements, and  $BP$  and  $RP$  are the *Gaia* magnitude measurements.

The residual of each variable with respect to its linear fit is normalized by the IQR of the residual's distribution. The IQR value is chosen over the standard deviation to avoid the influence of outliers, which are numerous in the relationship (as shown in Figure 5). Including the normalization coefficient, the Euclidean distance of each data point is then:

$$d_i = \sqrt{\left(\frac{\theta_i - \hat{\theta}_i}{\text{IQR}_\theta}\right)^2 + \left(\frac{Zg_i - \hat{Zg}_i}{\text{IQR}_{Zg}}\right)^2 + \left(\frac{Zr_i - \hat{Zr}_i}{\text{IQR}_{Zr}}\right)^2} \quad (7)$$

in which  $\text{IQR}_\theta$ ,  $\text{IQR}_{Zg}$ , and  $\text{IQR}_{Zr}$  are  $0.113''$ ,  $0.056$  mag, and  $0.112$  mag, respectively. As displayed in Figure 6, the distribution of  $d$  has a peak at  $d \approx 2$  and then falls off. It also shows outliers for  $d > 10$ , that we exclude by imposing a conservative threshold at  $d = 8$ , which removes possible wrong cross-matches. This excludes 30 outliers, whose positions in the multi-dimensional space are marked in Figure 5. Finally, we obtain 864 good cross-matches from the ZTF query results. We are aware that by using magnitudes as cross-match criteria, we may remove cataclysmic variable sources. However, this should not exclude periodic sources such as pulsating stars or binary stars, which are the main focus of this study.

### 4.2. Cleaning ZTF light curves

After selecting good cross-matches, in the next step, we employ the ZTF flags recommended by Guidry et al. (2021) to remove contaminated measurements in each ZTF time series. Specifically, we require good ZTF photometry measurements to follow these three criteria:

$$\begin{aligned}\text{catflag} &= 0 \\ |\text{sharp}| &< 0.25 \\ \text{mag} &< \text{limitmag} - 1.0.\end{aligned}\quad (8)$$

Having performed this preliminary cleaning, we then apply a  $5\sigma$  clipping selection aiming to remove the potential remaining outliers. Indeed, we observed that, for some ZTF light curves, simply applying the criteria outlined in (8) did not suffice to exclude probable outliers.

### 4.3. Period search methodology

We then analyze our cleaned time series with Generalised Lomb-Scargle periodograms (introduced by Lomb

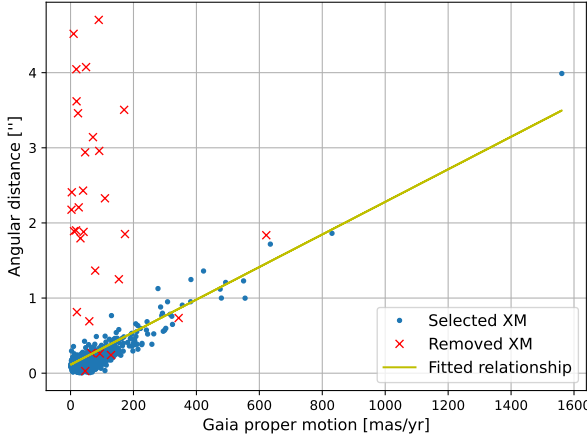
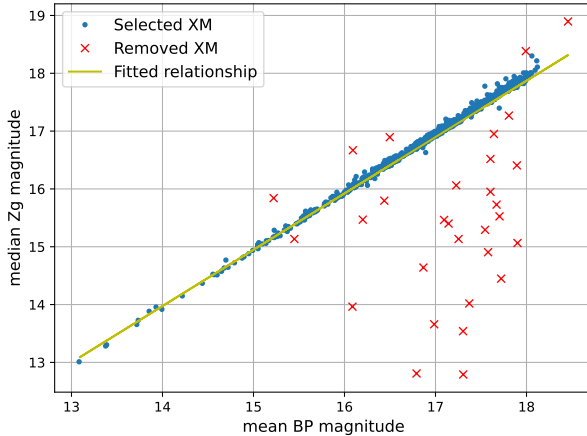
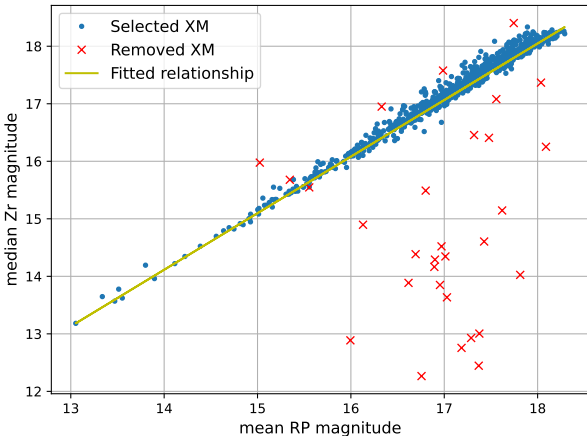
(a) *Gaia* proper motion vs angular distance.(b) *Gaia* BP mag vs Zg mag.(c) *Gaia* RP mag vs Zr mag.

Fig. 5: Inconsistent cross-matches of the ZTF query are detected and removed by comparing the astrometric and photometric measurements between *Gaia* and ZTF in the multi-dimensional space.

1976; Scargle 1982). In particular, we use the `Astropy` (Astropy Collaboration et al. 2018, 2022) implementation of the multi-band periodogram (developed by VanderPlas & Ivezić 2015), scanning frequencies ranging from  $f = 0$  to  $f = 0.5 \text{ min}^{-1}$  ( $= 720 \text{ day}^{-1}$ ), with an oversampling factor  $n_0 = 10$ .

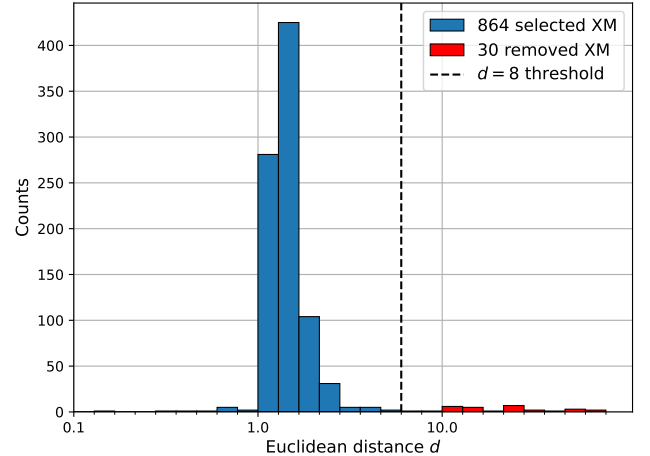


Fig. 6: The distribution of the Euclidean distance - as calculated in Equation (7) - of all our cross-match query. Good cross-matches should have  $d$  closer to 0. We remove those with  $d$  larger than 8.

Furthermore, we use  $(N_{\text{base}}, N_{\text{band}}) = (1, 0)$ , focusing our search on periodic variations common to both bands. This choice was made as it significantly decreases computation time. Indeed, as our targets can have long observational baselines ( $\gtrsim 6$  years), computing the periodogram with a well-defined frequency grid can require up to  $N_{\text{eval}} \sim 10^6$  evaluations, and adding a base term ( $N_{\text{base}} > 0$ ) increases computation time by a factor 60 (from  $\sim 1$  min to  $\sim 1$  h). Additionally, we compute the false-alarm probability at the extracted peak frequency in both bands (rather than in the multi-band periodogram, as it has not been implemented) using the Baluev upper limit (Baluev 2008). An illustration of this reduction process is displayed in Figure 7. We then select stars as variables of frequency  $f$  by imposing the following criteria:

$$\begin{aligned} FAP_{Zg \text{ resp. } Zr}(f) &< 10^{-3} \\ FAP_{Zr \text{ resp. } Zg}(f) &< 10^{-2} \\ LS(f) &> 0.1 \end{aligned} \quad (9)$$

With  $FAP_\alpha(f)$  being the false alarm probability of a signal at frequency  $f$  in the band  $\alpha$ , and  $LS(f)$  the multi-band Lomb-Scargle power at frequency  $f$ . The last criterion ( $LS(f) > 0.1$ ) allows us to exclude peaks caused by very noisy signals. Furthermore, we perform a visual check of the phase-folded light curves and periodogram in the cases where  $|f \bmod 1.00274 \text{ day}^{-1}| < 10^{-2}$  - i.e. if the resulting frequency is close to one cycle per sidereal day or an alias, hinting towards a windowing effect from the daily observations - or  $LS(f) < 0.25$  (underlying a noisy signal). Furthermore, in the cases where  $|f \bmod 1.00274 \text{ day}^{-1}| < 10^{-2}$ , we apply the periodogram to the *Gaia* light curves (if they are available), to confirm or exclude the periodicity.

Out of our 864 candidates, we confirm 141 (16%) periodic variables, 7 (1%) undetermined variables (variable stars for which we could not determine a pulsation frequency), and 716 (83%) stars for which no determined variability. This significant size of the last group can be traced back to two main reasons:

- Our selection criteria on the Lomb-Scargle analysis, outlined in Eq. (9) is possibly too harsh, in particular the Lomb-Scargle power cut  $LS(f) > 0.1$ , as it can exclude stars with

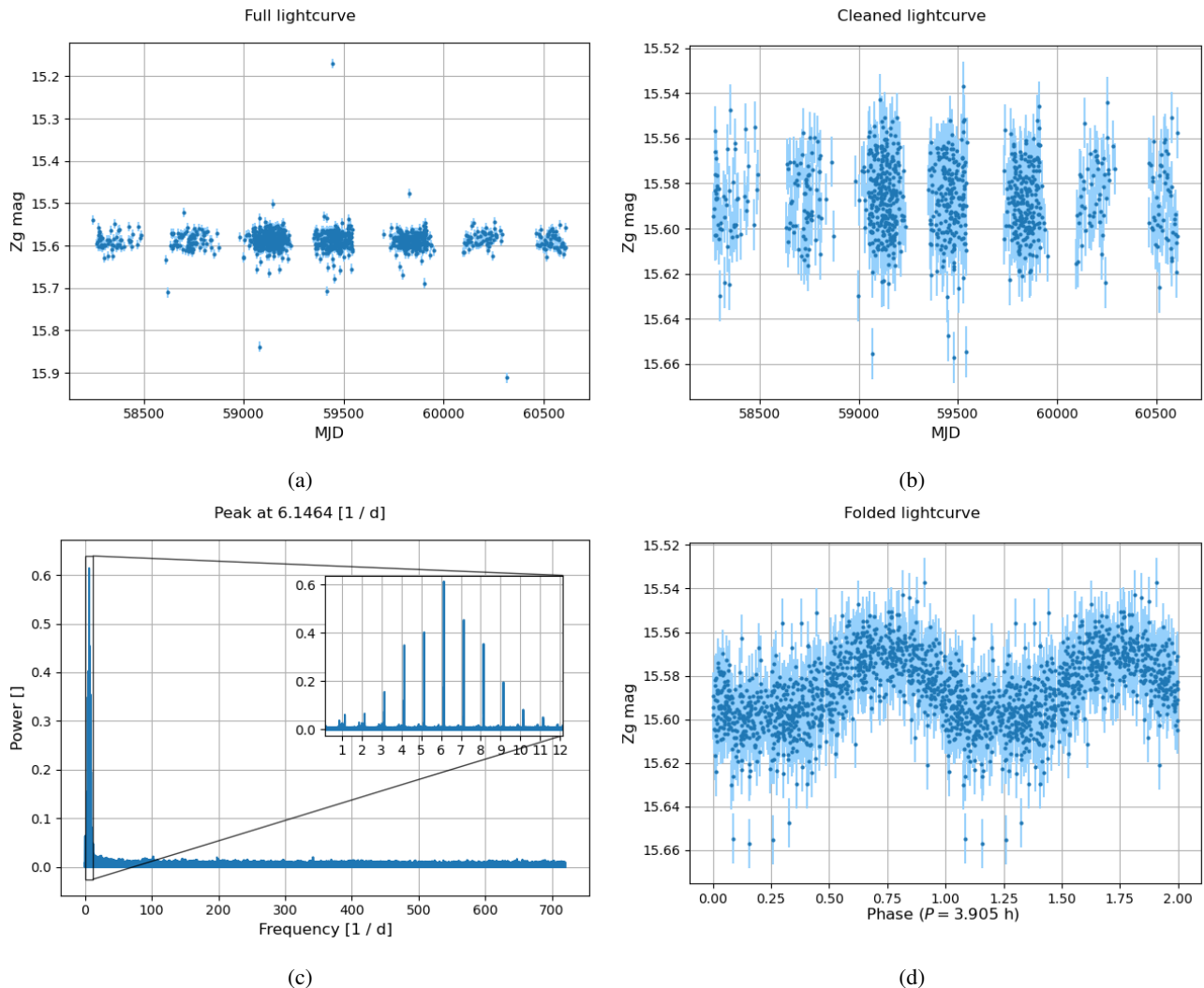


Fig. 7: We illustrate the step-by-step reduction of a raw ZTF DR23 light curve (of Gaia DR3 2833849800205759360) into a phase-folded light curve. Between (a) and (b), outlier observations are removed from the raw data using the procedure described in §4.2. In this case, 93 of the 1067 initial measurements were flagged as outliers. The cleaned light curve is then examined (c) using a multiband Lomb-Scargle periodogram (here with a peak at 6.1464 cycles per day). In (d) we present a folded light curve using the determined period.

high frequencies (which usually yield a lower peak power value) and stars with low amplitude-to-noise ratio (which induces spurious peaks and reduces the peak power value).

- This study focuses on checking whether some white dwarfs present periodic variability rather than establishing if they are variable or not, thus these stars might still present some variability - especially given our strong candidacy criteria for variability in §3.1.

The location on the HR diagram of the periodic stars is displayed in Figure 8, along with their frequency, and amplitude ratio  $A_r/A_g$ . The amplitude in the  $\alpha$  band is defined as

$$A_\alpha = Q_{0.95}(\alpha) - Q_{0.05}(\alpha) \quad (10)$$

with  $Q_p$  the  $p$ -th quantile of the cleaned observations in a given band.

## 5. Periodic white dwarfs

### 5.1. Classifying periodic White Dwarfs

Following Althaus et al. (2010), the main groups of pulsating white dwarfs are the ZZ Ceti, V777 Her, GW Vir, and DQVs. Using automatic unsupervised clustering, we attempt to retrieve at least some of these groups in our sample of pulsating white dwarfs. In particular, we use `sklearn`'s implementation of the OPTICS clustering algorithm (see Ankerst et al. 1999; Schubert & Gertz 2018) with hyperparameter `min_samples` = 6. The parameters used for clustering are the stars' absolute G magnitude, BP-RP colour,  $\log_{10}$  frequency, and  $\log_{10}$  amplitude ratio ( $A_r/A_g$ ). We retrieve 3 clusters, totalling 82 classified and 57 unclustered stars. Furthermore, we perform a sanity check through visual inspection of Figure 8 to identify possible clusters, during which we identify the same 3 clusters, a fourth smaller one, and a lone isolated star.

The first consists of stars with  $A_r/A_g \gtrsim 1.5$  (indicated by the yellow-red colours) and  $f \lesssim 50 \text{ day}^{-1}$  lying above the white

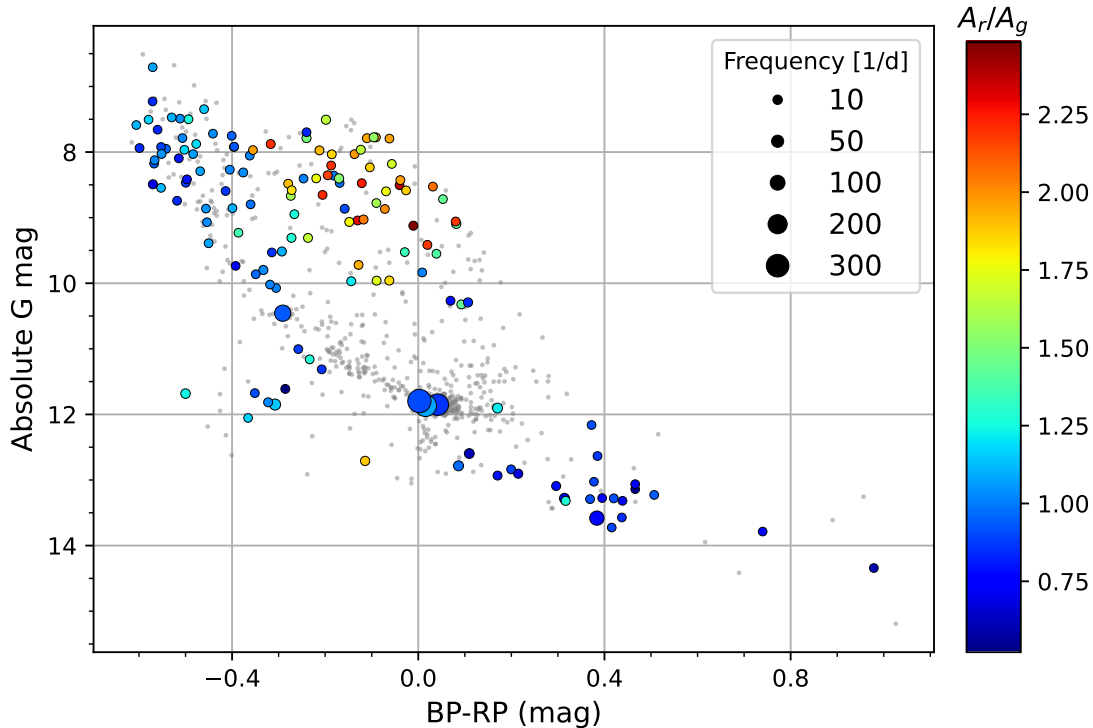


Fig. 8: Position of the determined periodic stars in the HR diagram, with the colour and size of the dots representing respectively their  $r/g$  amplitude ratios (see (10)) and frequency. The background grey dots represent the non-periodic stars in our candidate list.

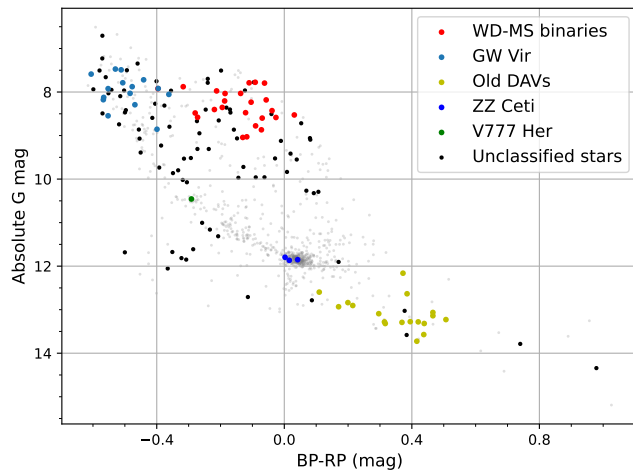


Fig. 9: Position in the HR diagram of the three clusters identified using unsupervised clustering, with the manually identified ZZ Ceti and V777 Her stars added. The background grey dots are the stars we found to be non-periodic.

dwarf sequence (absolute  $G < 10$  and  $BP - RP \in [-0.4, 0.1]$ ). These are presumed to be white dwarfs - main-sequence binary stars due to their high  $Zr$  amplitude.

The second group consists of blue ( $BP - RP \lesssim -0.4$ ) stars along the main white dwarf track, with  $f \lesssim 50 \text{ day}^{-1}$  and  $A_r/A_g \lesssim 1.25$ . We identify them as possible GW Vir stars. The third group corresponds to old variable white dwarfs, mostly DAVs, with absolute  $G > 12$ ,  $BP - RP > 0$ , an amplitude ratio between 0.75 and 1, and  $f < 100 \text{ day}^{-1}$ .

The small, visually identified, cluster consists of three high-

frequency ( $f > 200 \text{ day}^{-1}$ ) stars at absolute  $G \sim 11.5$  and  $BP - RP \sim 0.05$ . These are identified as ZZ Ceti stars due to their characteristic frequencies, position in the HR diagram, and amplitude ratios between 1 and 1.25. They were not clustered by the OPTICS algorithm, as they are too few to be recognised as a cluster. This raises a discrepancy between the visible over-density of the ZZ Ceti region on Figure 9 and the low number of identified periodic stars in the same region. We suspect this to be caused by the high frequency of ZZ Ceti stars (up to  $\sim 900$  cycles a day) - increasing the Lomb-Scargle periodogram's sensitivity to noise in the measurements. Furthermore, the detected ZZ Ceti stars'  $Zg$  and  $Zr$  amplitudes (respectively 86 millimag and 82 millimag) are approximately half those of the full sample (respectively 149 millimag and 186 millimag), further increasing the potential for spurious peaks in the periodograms and reducing the power value of a potential true frequency peak. Nevertheless, this outlines the significant potential to identify new ZZ Cetis in this region of the HR diagram in the future.

Finally, similarly as for the three ZZ Cetis, we identify a possible V777 Herculis star in the expected clump, at absolute  $G = 10.46$  and  $BP - RP = -0.22$  with a frequency  $f = 176.6 \text{ day}^{-1}$ , clearly in the range outlined by Althaus et al. (2010) for these kind of stars.

## 5.2. Stars to investigate

After visual inspections of the phase-folded light curves, we recommend the further investigations of at least 6 of our 141 periodic variables. These sources were selected as they present peculiar characteristics in their phase-folded light curves. In particular: Gaia DR3 103999471976858496 presents a peculiar bump, indicating secondary period, such as a transit; Gaia DR3 1191504471436192512 and Gaia

DR3 930093722208184448, both classified as WD-MS binaries, present characteristics of eclipsing binaries. The remaining 3, Gaia DR3 6770227729752288256, Gaia DR3 6844375121726139520, and Gaia DR3 4318508939464901760, present an intriguing "double band" feature in their Zr light curves. The 6 phase-folded light curves are provided as an appendix (see Figure A.1). Furthermore, we recommend further investigations for the 7 undetermined variables to determine their variability mechanism and potential periodicity.

### 5.3. Crossmatch with the MWDD

We cross-matched our catalogue of white dwarfs with the Montreal White Dwarf Database<sup>3</sup> (MWDD - introduced by Dufour et al. 2017), to compare how many of them are already known and classified, and to ascertain the quality of our classifications. Out of our 864 star sample, 345 are already present in the MWDD, with 65 of the 148 variable stars already classified, and 280 of the 716 non-variable. In particular, out of our 24 identified WD-MS binaries, 4 are already classified as such in the MWDD, for the GW Vir stars, 5 are already known out of 15, 2 of the 3 ZZ Cetis, 16 of the 18 old DAVs, and our lone V777 Her being previously classified too.

The result of this cross-match is listed in the *note* column of the data table resulting from this work (see Table A.1 for an excerpt of the table). The complete table will be provided as a companion to this paper on the well-known VizieR database<sup>4</sup> (introduced by Ochsenbein et al. 2000).

## 6. Conclusion

Using the photometric and astrometric measurements of *Gaia* DR3, we propose 1423 candidates for variable white dwarfs. Using a multiband Lomb-Scargle analysis on 864 candidates having ZTF DR23 time series, we confirm 148 variables, 141 of them being periodic (83 being newly identified). Using unsupervised clustering, we regroup them in 5 main groups, ZZ Ceti, GW Virginis, MS-WD binaries, Old DAVs and V777 Herculis; yielding 3 ZZ Ceti candidates, 15 GW Virginis candidates, 24 WD-MS binary systems, 18 Old DAVs and one V777 Herculis.

Furthermore, we compare our catalogue with the MWDD's, for previously identified sources, which yields 519 newly identified variable white dwarf candidates. Among these 519 newly identified candidates, we confirm 1 new ZZ Ceti, 10 new GW Virginis, 20 new WD-MS binary systems, and 2 Old DAVs.

A sample of our 864 ZTF-observed variable candidates, along with their classifications, frequencies, and amplitudes, is provided in Table A.1. The complete list of our candidates is provided as companion to the paper, on the VizieR database of the Centre de Données astronomiques de Strasbourg.

In the future, starting with *Gaia* DR4 (expected by the end of 2026), photometric time series will be available in all bands (G, BP, RP, and G\_RVS) as well as in radial velocities (for the bright part of the survey). The combination of *Gaia* data (astrometry, photometry, and radial velocities) with ZTF observations will enable detailed studies of white dwarf variability. In particular, aliasing issues will be mitigated thanks to the different spectral windows of the two surveys. These developments promise major progress in our understanding of variable white dwarfs.

**Acknowledgements.** We thank Richard I. Anderson, Anthony Brown, Boris Gaensicke, and Nami Mowlavi for discussions and comments. We thank also late

Prof. Gilles Fontaine for his encouragements at the beginning of this work. We also thank the ThinkSwiss Research Scholarship for financially support Thinh Nguyen to do research at the University of Geneva, and we thank the University of Geneva for their welcome and hospitality to the guest student. This work has made use of data from the European Space Agency (ESA) mission *Gaia* (<https://www.cosmos.esa.int/gaia>), processed by the *Gaia* Data Processing and Analysis Consortium (DPAC, <https://www.cosmos.esa.int/web/gaia/dpac/consortium>). Funding for the DPAC has been provided by national institutions, in particular the institutions participating in the *Gaia* Multilateral Agreement. This work is partly based on observations obtained with the Samuel Oschin Telescope 48-inch and the 60-inch Telescope at the Palomar Observatory as part of the Zwicky Transient Facility project. ZTF is supported by the National Science Foundation under Grants No. AST-1440341 and AST-2034437 and a collaboration including current partners Caltech, IPAC, the Oskar Klein Center at Stockholm University, the University of Maryland, University of California, Berkeley, the University of Wisconsin at Milwaukee, University of Warwick, Ruhr University, Cornell University, Northwestern University and Drexel University. Operations are conducted by COO, IPAC, and UW. This research also made use of the NASA/IPAC Infrared Science Archive, which is funded by the National Aeronautics and Space Administration and operated by the California Institute of Technology, the VizieR catalogue access tool, CDS, Strasbourg Astronomical Observatory, France, and the Montreal White Dwarf Database.

## References

Althaus, L. G., Córscico, A. H., Isern, J., & García-Berro, E. 2010, A&A Rev., 18, 471  
 Ankerst, M., Breunig, M. M., Kriegel, H.-P., & Sander, J. 1999, SIGMOD Rec., 28, 49  
 Astropy Collaboration, Price-Whelan, A. M., Lim, P. L., et al. 2022, ApJ, 935, 167  
 Astropy Collaboration, Price-Whelan, A. M., Sipőcz, B. M., et al. 2018, AJ, 156, 123  
 Baluev, R. V. 2008, Monthly Notices of the Royal Astronomical Society, 385, 1279  
 Bellm, E. C., Kulkarni, S. R., Graham, M. J., et al. 2019, PASP, 131, 018002  
 Belokurov, V., Erkal, D., Deason, A. J., et al. 2017, MNRAS, 466, 4711  
 Dufour, P., Blouin, S., Coutu, S., et al. 2017, The Montreal White Dwarf Database: A Tool for the Community, conference Name: 20th European White Dwarf Workshop Volume: 509 ADS Bibcode: 2017ASPC..509....3D  
 Evans, D. W., Riello, M., De Angeli, F., et al. 2018, A&A, 616, A4  
 Eyer, L. 1998, PhD thesis, University of Geneva  
 Eyer, L., Audard, M., Holl, B., et al. 2023, A&A, 674, A13  
 Eyer, L., Mowlavi, N., Evans, D. W., et al. 2017, arXiv e-prints, arXiv:1702.03295  
 Eyer, L., Rimoldini, L., Rohrbasser, L., et al. 2020, in Stars and their Variability Observed from Space, ed. C. Neiner, W. W. Weiss, D. Baade, R. E. Griffin, C. C. Lovekin, & A. F. J. Moffat, 11–17  
 Gaia Collaboration, Brown, A. G. A., Vallenari, A., et al. 2018, A&A, 616, A1  
 Gaia Collaboration, Brown, A. G. A., Vallenari, A., et al. 2021, A&A, 649, A1  
 Gaia Collaboration, Brown, A. G. A., Vallenari, A., et al. 2016a, A&A, 595, A2  
 Gaia Collaboration, Eyer, L., Rimoldini, L., et al. 2019, A&A, 623, A110  
 Gaia Collaboration, Prusti, T., de Bruijne, J. H. J., et al. 2016b, A&A, 595, A1  
 Gaia Collaboration, Vallenari, A., Brown, A. G. A., et al. 2022, arXiv e-prints, arXiv:2208.00211  
 Gentile Fusillo, N. P., Tremblay, P. E., Cukanovaite, E., et al. 2021, MNRAS, 508, 3877  
 Gentile Fusillo, N. P., Tremblay, P.-E., Gänsicke, B. T., et al. 2019, MNRAS, 482, 4570  
 Guidry, J. A., Vanderbosch, Z. P., Hermes, J. J., et al. 2021, ApJ, 912, 125  
 Lindegren, L., Hernández, J., Bombrun, A., et al. 2018, A&A, 616, A2  
 Lindegren, L., Klioner, S. A., Hernández, J., et al. 2021, A&A, 649, A2  
 Lomb, N. R. 1976, Ap&SS, 39, 447  
 Maíz Apellániz, J., Holgado, G., Pantaleoni González, M., & Caballero, J. A. 2023, A&A, 677, A137  
 Masci, F. J., Laher, R. R., Rusholme, B., et al. 2018, Publications of the Astronomical Society of the Pacific, 131, 018003, publisher: The Astronomical Society of the Pacific  
 Mignard, F., Bailer-Jones, C., Bastian, U., et al. 2008, in IAU Symposium, Vol. 248, A Giant Step: from Milli- to Micro-arcsecond Astrometry, ed. W. J. Jin, I. Platais, & M. A. C. Perryman, 224–230  
 Mowlavi, N., Rimoldini, L., Evans, D. W., et al. 2021, A&A, 648, A44  
 Ochsenbein, F., Bauer, P., & Marcout, J. 2000, Astronomy and Astrophysics Supplement Series, 143, 23  
 Riello, M., De Angeli, F., Evans, D. W., et al. 2021, A&A, 649, A3  
 Rimoldini, L., Holl, B., Gavras, P., et al. 2023, A&A, 674, A14

<sup>3</sup> <https://www.montrealwhitedwarfdatabase.org/home.html>

<sup>4</sup> <https://cdsarc.u-strasbg.fr/>

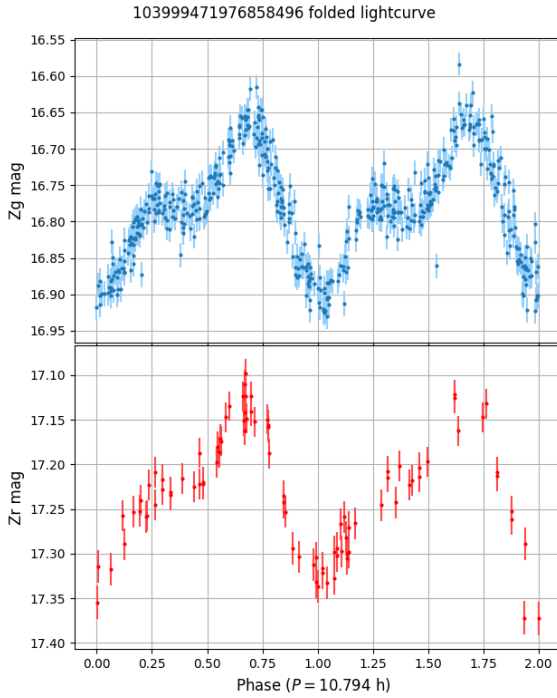
Scargle, J. D. 1982, *ApJ*, 263, 835

Schubert, E. & Gertz, M. 2018, in *CEUR Workshop Proceedings*, Vol. 2191, *Proceedings of the Conference "Lernen, Wissen, Daten, Analysen"*, ed. R. Gemulla, S. P. Ponzetto, C. Bizer, M. Keuper, & H. Stuckenschmidt (Mannheim, Germany: CEUR), 318–329, iSSN: 1613-0073

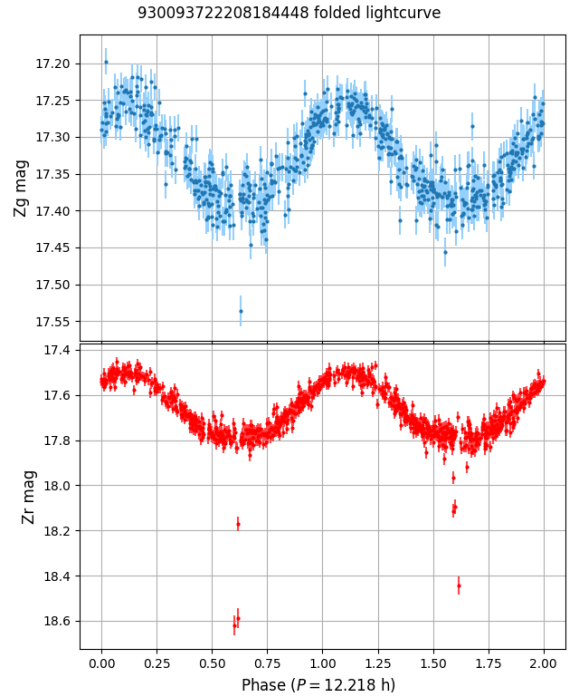
VanderPlas, J. T. & Ivezić, Ž. 2015, *The Astrophysical Journal*, 812, 18, publisher: IOP ADS Bibcode: 2015ApJ...812...18V

Virтанен, P., Гоммерс, Р., Олифант, Т. Е., et al. 2020, *Nature Methods*, 17, 261, publisher: Nature Publishing Group

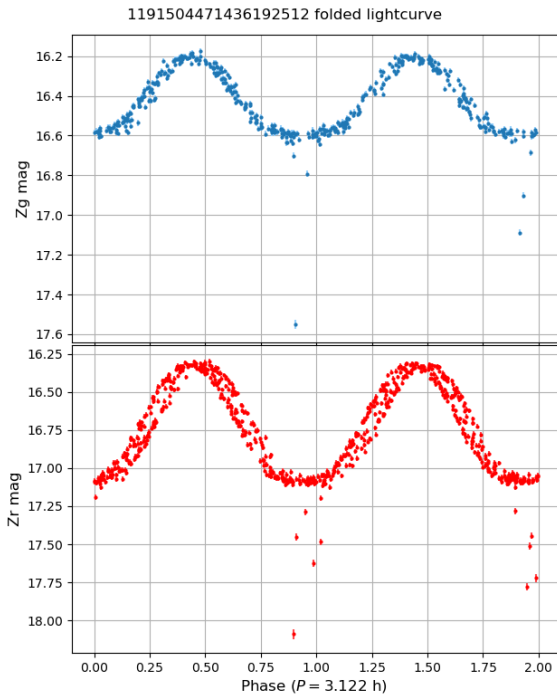
## **Appendix A: Additional materials**



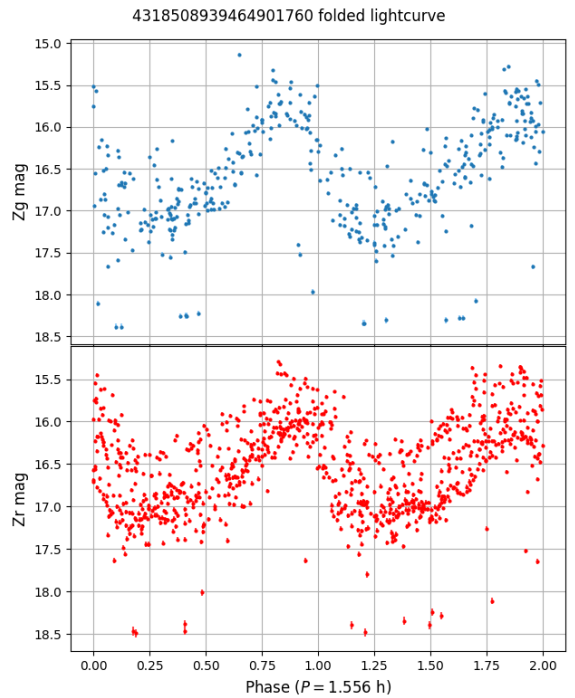
(a) Gaia DR3 103999471976858496



(b) Gaia DR3 930093722208184448



(c) Gaia DR3 1191504471436192512



(d) Gaia DR3 4318508939464901760

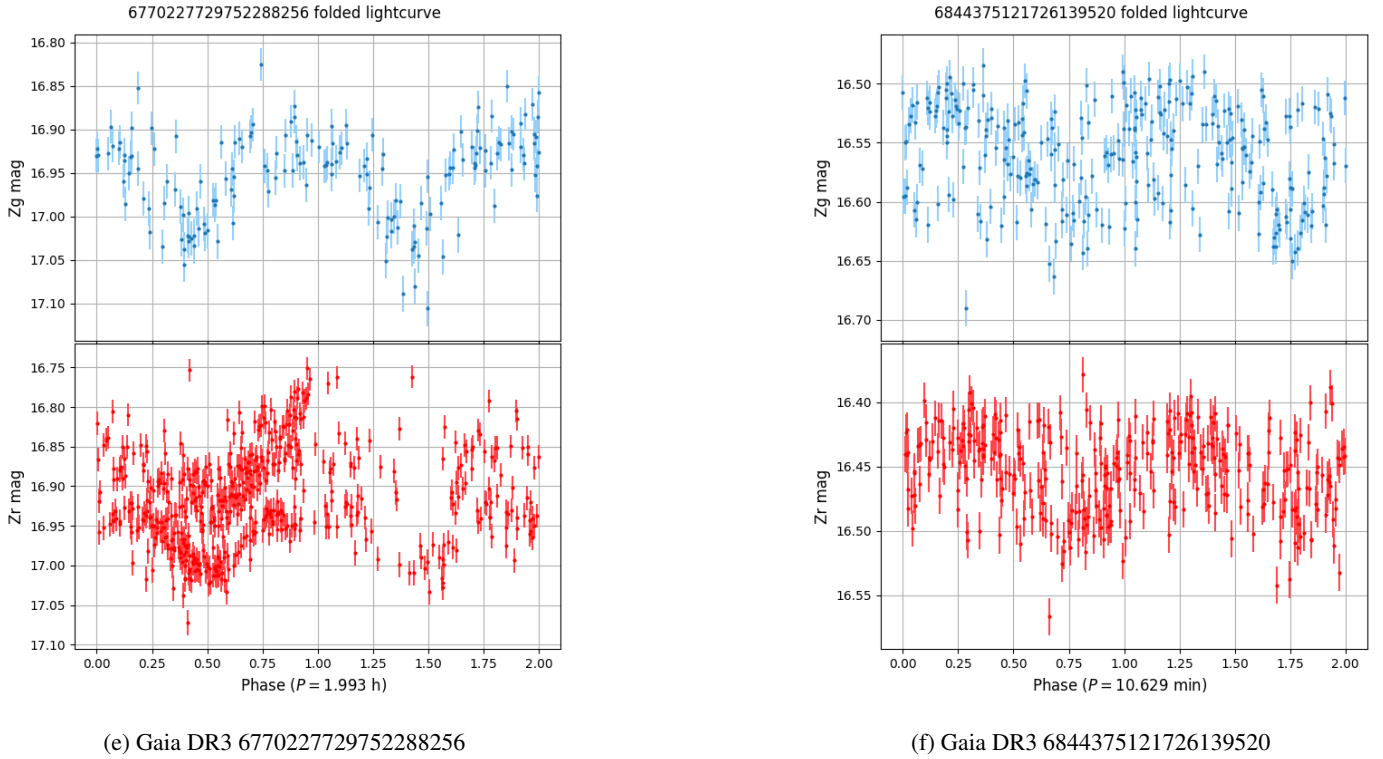


Fig. A.1: Phase-folded light curves of the 6 periodic sources warranting further investigations.

Table A.1: Excerpt of the companion table

WDJname	GaiaDR3_id	ra	e_ra	dec	e_dec	plx	e_plx	G_mag	RP_mag
WDJ135309.97+484021.17	1510467090935595008	208.29	0.04	48.67	0.04	5.7	0.05	16.68	16.88
WDJ052038.32+304823.92	3446909137068558464	80.16	0.04	30.81	0.02	17.51	0.04	15.58	15.59
WDJ111026.19+191229.75	3984115430179696128	167.61	0.09	19.21	0.07	16.65	0.1	17.17	16.91
WDJ070223.05-174931.25	2935237657195591424	105.6	0.04	-17.83	0.05	1.81	0.06	16.51	16.55
WDJ220247.69+275010.67	1893101535448502400	330.7	0.05	27.84	0.07	2.23	0.07	16.55	16.86
WDJ105010.80-140436.76	3750072904055666176	162.54	0.08	-14.08	0.06	9.15	0.09	17.14	17.09
WDJ143406.77+150817.81	1228266814506156928	218.53	0.04	15.14	0.03	12.68	0.04	16.01	16.09
WDJ024849.59+264332.15	114808397128552576	42.21	0.11	26.73	0.15	5.67	0.11	17.23	17.34
WDJ163914.29+474835.84	1410345596469085184	249.81	0.07	47.81	0.07	6.71	0.08	17.76	17.78
WDJ022917.15-150350.42	5146019876066016000	37.32	0.08	-15.06	0.08	5.48	0.1	17.71	17.63
WDJ220420.60+282321.36	1893512958955407232	331.09	0.08	28.39	0.08	5.27	0.1	17.74	17.67

BP_mag	g_mag	r_mag	Variable	Periodic	frequency	g_amp	r_amp	classification	note
16.59	16.54	16.92	True	True	176.58	0.11	0.1	V777 Her	registered in MWDD
15.59	15.53	15.73	True	True	320.01	0.07	0.06	ZZ Ceti	registered in MWDD
17.33	17.35	17.2	True	True	5.38	0.13	0.12	Old DAVs	
16.44	16.49	16.89	True	True	8.82	0.28	0.55	WD-MS binaries	
16.39	16.38	16.89	True	True	1.23	0.06	0.06	GW Vir	
17.2	17.09	17.17	True	False	0.0	0.31	0.48		Further analysis recommended
15.99	15.9	16.17	False	False	0.0	0.0	0.0		registered in MWDD
17.19	17.09	17.39	False	False	0.0	0.0	0.0		
17.81	17.72	17.9	False	False	0.0	0.0	0.0		
17.8	17.71	17.79	False	False	0.0	0.0	0.0		
17.86	17.77	17.86	False	False	0.0	0.0	0.0		